

Computational Study and Analysis of the Optical Fiber Tip Mechanical Damage Threats during Laser Surgical Operations

Munqith S. Dawood

Medical engineering department

Collage of engineering

Al-Nahrain University

E-mail: monkithsdz51@yahoo.com

Abstract:

The damage of optical fiber tips during medical surgical applications of lasers in a liquid environment were noticed in arthroscopic and lithotripsy operations. The phenomenon of the laser produced cavitation bubbles and their collateral mechanical effects on the delivery fiber tip during these operations are studied. It was found that the optical fiber tip is subjected to the threats of the bubbles collapse transient pressures and to the strikes of the produced hammering jets beside the shearing forces due to the high speed bubbles flow. These frequently repeated mechanical forces are calculated for three different sizes of optical fibers. The results showed that to minimize the damage effects of these forces, it is preferable to use the smaller diameter of 200 μm fiber, beside holding the fiber tip at about 5-7 mm away from the treated tissue or calculi targets during the operation to prolong its operating life and in the same time maintaining the efficient ablation.

Keywords: optical fiber damage; cavitation bubbles; bubbles dynamic; hammer jet.

Nomenclatures

C_u	shock wave velocity in the saline ≈ 1489 , m/s;
E_b	energy of the bubble;
F_{sh}	shearing force;
K	acquired kinetic energy;
P_{ext}	external pressure = 1.013 bar = 10^5 pa;
P_o	hydrostatic pressure;
P_v	vapor pressure;
r	spherical radial coordinate of a point external to the bubble;
r_j	jet tip radius;
R	spherical radial coordinate of a point external to the bubble;
R_{bi}	bubble initial radius;
R_{bmax}	maximum expanded radius of the bubble;

R_f	optical fiber radius;
t	bubble expansion time;
U_r	bubbles radial flow;
V	specific volume;
W	work done by the bubble on the external fluid;
Z	absorption length of the laser light;
δ	distance between the bubble wall and the rigid body (stone, tissue or the fiber tip).
λ	dynamic viscosity of the saline;
ρ	saline density;
τ_h	time (μs);
ΔP	change in pressure due to the bubble motion;
t_c	collapse time;
P_h	water hammer pressure;
U_{Rb}	bubble growth rate.

1. Introduction

The optical fibers are widely used in different medical and surgical applications such as in arthroscopic and lithotripsy operations to deliver lasers usually within the 1.9-3 μm band of wavelengths to the required tissue or calculi targets. The most common types of these lasers are the Thulium fiber (1.908 μm), Ho:YAG (2.120 μm), and the Er:YAG laser (2.94 μm). Usually the pulse duration of these lasers governs the dominant mechanism of the target ablation, which is either photothermal or photoacoustic (photomechanical).

The long laser pulse durations ($>10 \mu\text{s}$) induce a temperature rise in the laser-affected zone with minimal acoustic waves. In this case the target material is removed by means of vaporization, melting, mechanical stress, and/or chemical decomposition [1].

The ablation by using short-pulsed laser ($< 10 \mu\text{s}$) mainly has mechanical phenomena due to the creation of plasma at the stone surface, which results in the cavitation bubbles development [1,2].

These operations are carried out under the direct vision by using small flexible endoscopes to ablate the target tissues or calculi which are flushed with sterile saline solution.

In case of contact laser ablation, the produced high temperature rise creates plasma followed by the emission of pressure transient and cavitation bubbles generation.

When the fiber tip is not in contact with the tissue or the stone, the principal operation is based on the transformation of the high energy pulsed laser light into cavitation vapor bubbles, which are produced by the strong absorption of the laser energy in the flushed saline solution separating the fiber tip and the tissue surface [2,3]. During the operation, the treated target and the fiber tip are both subjected to many physical effects collateral to the laser irradiation, like the plasma formation, rapid thermal expansion, the generation of vapor bubbles, the bubbles collapse pressure shock waves dynamics and the high speed flow [3].

All of these events have their disruption effects not only on the ablation area but on the optical fiber tip face also.

The damage of the end tip of the fiber decreases the clinical and surgical process efficiency due to the defocusing and the deformation of the power distribution within the laser spot out of the damaged optical fiber. In addition, the remaining quartz splinters of the cracked fiber in the treated organ tissues after laser treatment can cause further tissue damage and other complications. Beside its compatibility and optical parameters, the optimum selection of the optical fiber should consider its high damage threshold and even the geometrical shape of the its end tip and the core-cladding whether it is conventional or short tapered [4].

2. Methods

2.1. Bubbles dynamics and scaling models

The delivered laser energy will generate the almost spherical shape bubbles in case of using moderate laser fluencies. The large pressure in the laser-induced vapor bubble leads to a very rapid expansion that overshoots the equilibrium state, in which the internal bubble pressure equals the hydrostatic pressure, then the expansion stops. The energy E_b of the bubble is directly proportional to the cubic of its maximum expanded radius R_{bmax} and to the pressure difference Δp between the hydrostatic pressure P_o and the vapor pressure P_v , inside the bubble as explained by eq.(1) [5,6, 7]:

$$E = \frac{4}{3}\pi(P_o - P_v)R_{bmax}^3 \dots\dots(1)$$

A very interesting feature of the bubble growth was observed experimentally by T. Asshauer et.al. [3,8]. Their experiments showed that at high laser

fluencies, the generated bubbles will have an elongated, pear shape or cylindrical shape rather than the symmetrical spherical shape. This shape deformation leads to decrease of the inside bubble pressure and it may disintegrate the bubble into two distinct parts. One of these parts is the proximal part, which is centered on the fiber tip end and has a quasi-spherical form. The other part is the distal cylindrical shape part. Due to the still in progress liquid vaporization along the axis of the fiber tip, a complete collapse of the proximal bubble part is reached while the distal part of the bubble collapses later after few hundreds of micro seconds with weaker transient pressure. These multi-center bubbles produce weaker collapsing pressure than the spherical bubbles do.

Experiments done by R. A. London et.al. [9] showed also that the relatively short laser pulses produce larger bubbles than the long pulses did for the same specific energy deposition. For the same used laser fluency the generated bubble sizes will be proportional to the fiber diameter $2R_f$, this means that the smaller fiber cores generate smaller bubbles and consequently lower induced transient collapse pressures.

For a certain laser energy the initial radius R_{bi} of the induced cavitation bubble is related to the size of the fiber as shown in eq. (2). This equation based on the assumption that the initial volume of the bubble equals to the volume into which the laser energy is deposited in the liquid environment (or the tissue) by the optical fiber tip [9, 10, 11]:

$$R_{bi} = \sqrt[3]{\frac{3}{4}Z_a R_f^2} \dots\dots(2)$$

Where, Z_a is the absorption length of the laser light in the environment in front of the fiber tip face. It is equal to the reciprocal of its absorption coefficient μ_a .

According to Rayleigh equation, the cavitation bubble expands up to its maximum expected radius R_{bmax} in the liquid of density ρ according to the difference between the static and vapor pressures as follows in eq.(3)[7]:

$$R_{bmax} = \frac{t_c}{0.915} \sqrt{\frac{\rho}{\rho_o - \rho_v}} \dots\dots(3)$$

Where, t_c is the collapse duration, which is the time between the first bubble maximum and its subsequent minimum.

The expanded bubbles will flow toward their target and collapse after reaching their maximum diameter (4 – 8 mm) due to the static pressure of the surrounding fluid. A strong pressure transient appears during the collapse phase, which propagates in spherical wave shapes with a reciprocal dependency on the distance from the collapse center. Then a rebound phase of the

compressed bubble starts and the bubble expands again up to a smaller new R_{bmax} . The details of shock wave emission and bubble generation depend not only on the energy deposition mechanism, but also on its time scale and the degree of stress confinement [12, 13].

The very short interaction time of these multi induced shock waves with the tissue or the urinary stone lead to macroscopic disruption especially for high power shock waves [14].

Considering the condition of energy balance and assuming that the work done by the bubble on the external fluid is W , then the formula of the acquired kinetic energy K , will be as follows [8,9]:

$$K = 2\pi\rho \left(\frac{dR_b}{dt}\right)^2 \cdot R_b \dots\dots (4)$$

$$W = \int (P_v - P_{urine}) dV \dots\dots(5)$$

V is the specific volume.

Equating eqs.(4) and (5) gives the following relation between the bubble radius R_b and its expansion time, t :

$$t = \sqrt{2\pi\rho} \cdot \int_{R_{bo}}^{R_b} \sqrt{\frac{R_b^2}{W}} \cdot dR_b \dots\dots(6)$$

According to equation (6), for short laser pulses, R. A. London et.al. [9], showed that the cavitation bubble of initial radius R_{bi} expands during time t as shown in the simple eq.(7). Then the bubble reaches its maximum radius R_{bmax} at time t_{max} , after that it collapses and starts the rebound phase.

$$t = \sqrt{\frac{\rho}{P_{ext}}} \cdot R_{bi} \dots\dots(7)$$

Where:

ρ is the density of the saline solution = 1004.6 kg/m³;

$P_{ext} = 1.013 \text{ bar} \approx 10^5 \text{ pa}$.

After two or three collapse-rebound phases the bubble finally dissolves into micro bubbles.

The bubbles collapse transient pressure was measured practically by Asshauer et.al group [8]. They used a hydrophone pressure sensor to measure the bubbles collapse transient pressure produced by the 2.12 μm , CTH:YAG laser operating in water. They reported that the measured pressure at distance 4 mm away from the collapse center is 180 bar and about 3600 bar at 150 μm from the center. It is important to notice that whenever the pressure is coming from a high impedance zone and propagates into a zone of smaller impedance it is partially reflected as a tensile stress wave. These waves have a high damage potentials.

During the bubbles motion some momentum changes will appear in the liquid, which are corresponding to the pressure gradients. This means

that the motion of a bubble towards a rigid body will (radiate) pressure on the face of this rigid body (target or fiber face). Such pressure is gradually changing as shown in eq. (8) [14]:

$$\frac{\Delta P}{\rho} = \left[\frac{R_b^2}{\delta} \cdot \frac{d^2 R_b}{dt^2} + \frac{3R_b}{\delta} \cdot \left(\frac{dR_b}{dt}\right)^2 - \frac{R_b^2}{\delta^2} \cdot \left(\frac{dR_b}{dt}\right)^2 \right] \frac{R_b}{r} - \left[\frac{R_b^2}{2\delta^2} \cdot \left(\frac{dR_b}{dt}\right)^2 \right] \frac{R_b^4}{r^4} \dots\dots(8)$$

Where:

ΔP is the change in pressure due to the bubble motion;

ρ is the saline solution density;

δ is the distance between the bubble wall and the rigid body (stone, tissue or the fiber tip);

r is the spherical radial coordinate = $\delta + R_b$;

$r \approx R_b$ for very short distance of δ .

2.2 Jets and counterjets

For short distances between the bubble and the target, the pressure gradient ΔP becomes large. Consequently the compressed bubble will either produce jet effects or flow with high radial velocity as a flush stream on the face of the target producing pits or cracking shearing forces on it. The generated bubbles exclude the saline water around them and when they exist near a surface (tissue, calculi or fiber face), the excluded saline converges on a point, conserving the momentum given by the vapor bubbles generation during the bubbles collapse. This convergence increases the stagnation pressure of the point resulting in a large deformation of the bubbles surface near this point and leading to the formation of saline high speed jets [12]. All these events of bubbles generation, their flow, bubbles collapse and the jets formations during the laser operation create different pressure zones in different directions. They have their damage effects on the target and the possibility to force part of these bubbles to move towards the fiber tip and to be compressed on its face.

If the distance between the cavitation bubble and the target stone or tissue is further decreased a counterjet is formed, which points away from the target [15, 16].

The interaction of the shock waves with the vapor bubbles also create jets. The damage due to the shock wave alone could be ignored compared with the damage due to the interaction of a bubble with the shock wave when this bubble is attached to the target surface or to the fiber tip face. The configuration of the jet is nearly conical with a slightly rounded nose. Its radius is about 1/10 of the initial bubble radius [17,18]. This means that its effect is proportional to the bubble radius, which is in its role proportional to the fiber radius for a fixed laser energy.

When the bubble interacts with the rebound shock wave during the penetration of the forward jet into the target, it returns back to the upper stream to act as another source of counterjet formation. The counterjet could be generated also whenever the bubble initiated between two parallel rigid walls like the target surface and the fiber tip face. In this case an annular flow is developed during bubble collapse. For a sufficient distance between the two walls, an annular flow will be developed and leads to bubble splitting and the formation of two opposing liquid jets directed one towards the target and the other towards the fiber tip face [12,19].

In their experiments, T. Kodama and Y. Tomita in [20] used the Imacon 790 high speed camera and xenon flash lamp to photograph and record the collapsing bubbles behavior. By analyzing their imaging results in this paper, it is seen that when the distance between the fiber tip and the stone is more than 1.6 of the maximum expected bubble radius R_{bmax} , then only a shock wave impact will be produced on the face of the target stone or tissue. If the distance is less than this value, then the bubble will contact the target surface during the expansion phase and producing jet.

The jets have been shown to cause collateral damage effects and to increase the material removal or target fragmentation. Their damage range is slightly larger than the R_{bmax} [15,16]. The counterjet together with the transient shock waves will compress the existing bubbles in the vicinity of the fiber tip causing the undesired damage to its face especially after multiple repetitions of this phenomena. The generation of these inward jets and counterjets increased when the fiber end operates very close to the target and in the same time too much close to the collapse centers.

The jets may propagate by velocities of 35-69 m/s [12] and more up to 960 m/s [16]. These velocities increase due to the effects of the other bubbles collapse.

2.3 Hammer jet

The jet concentrates the bubble energy in the direction of its ejection flow by very high velocities toward the target to be ablated, producing very high concentrated water hammer pressure P_h up to 2000 bar. This disruptive pressure is directly proportional to the jet velocity V_j as follows [20]:

$$P_h \approx V_j \cdot \rho \cdot C_u \quad \dots\dots (9)$$

Where:

ρ is the saline density; and

C_u is the shock wave velocity in the saline.

According to [3,12,20] and considering the ambient vapor temperature effect, the shock wave velocity in the saline was considered to be 1489 m/s. The duration of the hammer jet pressure prolongs for a short microseconds time τ_h :

$$\tau_h \approx \frac{r_j}{C_u} \quad \dots\dots (10)$$

Where:

r_j = jet tip radius \approx 0.1 of the initial bubble radius R_{bi} .

The duration of the hammer jet is related to the bubble size, which is practically related to the used optical fiber radius and the applied laser energy. The repeated bubbles collapse transient pressure with the hammering actions on the fiber face have their pitting effect, which makes its surface rough and thus reduces the efficiency of the o/p laser beam [20].

When the fiber face is very close to the target, the bubbles will radially flow at high spherical radial velocity U_r calculated from eq.(11). The bubbles are flow along the target surface and along the fiber tip face as well [9,14]:

$$U_r = \frac{dR_b}{dt} \cdot \left(\frac{R_b}{r}\right)^2 \quad \dots\dots (11)$$

Where:

r is the spherical radial coordinate of a point external to the bubble;

dR_b/dt is the cavitation bubble growth.

This high radial velocity of bubbles and consequently fluid flow (flush) represents another effective fiber tip cracking damage source [9,14,20].

The velocity of the cavitation bubble growth rate is considered to be $U_{Rb} = dR_b/dt$. It is assumed to be uniform at $r \approx R_b$, nearby the fiber face, but as this radial distance increased i.e when $r \gg R_b$ then the flow of the bubble became spherically diverged.

By referring to the experimental works in [7,8,10,20] and analyzing their high speed camera images taken for the bubble collapse events, it was found out that the average bubble boundary velocity or the bubbles growth rate, dR_b/dt could be considered equal to 8 m/s. It depends on the used laser pulse duration and its energy.

The bubbles radial flow U_r is proportional to the bubbles sizes and produces tensile and shearing forces F_{sh} on the face of the fiber tip as explained by equation (12) [21]:

$$F_{sh} = \lambda \cdot \left(\frac{dU_r}{dr}\right) \quad \dots\dots (12)$$

Where: λ is the dynamic viscosity of the saline.

3. Results

According to eq. (2), the initial bubbles radii R_{bi} as a function of different optical fiber sizes (radii R_f) are shown in fig (1) for the Ho:YAG and Thulium fiber lasers. For simplicity, the absorption coefficients were considered linear and equal to 30 and 120 cm^{-1} for these two lasers respectively.

According to the experimental data and the high speed images presented in literatures [3,7,8], the dynamic sequence of the induced bubbles stages in saline was calculated in this paper and presented in sketch (1). Figure (2) shows the cavitation bubble expansion behavior, which was calculated from eq. (7).

The generated bubbles are flow mainly from the fiber side towards the target during the laser operation. The flow velocity was calculated by measuring the time at which the cavitation bubble collapses and their travelled distance during this

time. These measurements was carried out by analyzing and scaling the series of the Imacon 790 high speed camera image frames which appeared in [20]. The results of these calculations clarified that the bubbles are flow with a velocity of about 0.0224×10^6 mm/sec in average. Fig. (2) shows also that the bubble needs about 0.3 milliseconds to grow up to its average maximum radius (considered 3 mm). Then by simple calculations, it seems that during this time the cavitation bubble will pass a distance of 6.72 mm after its generation.

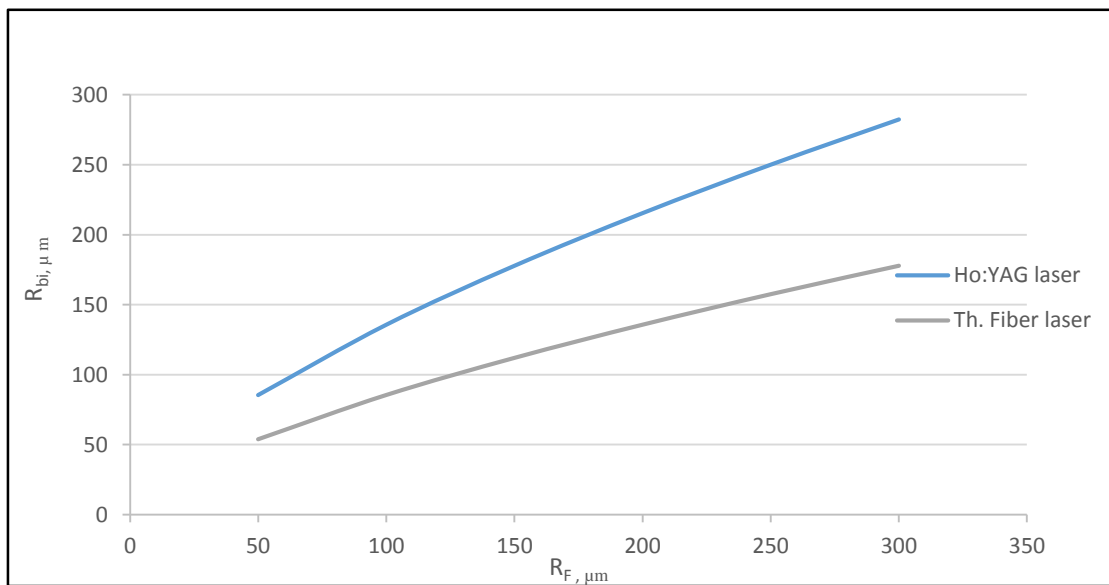
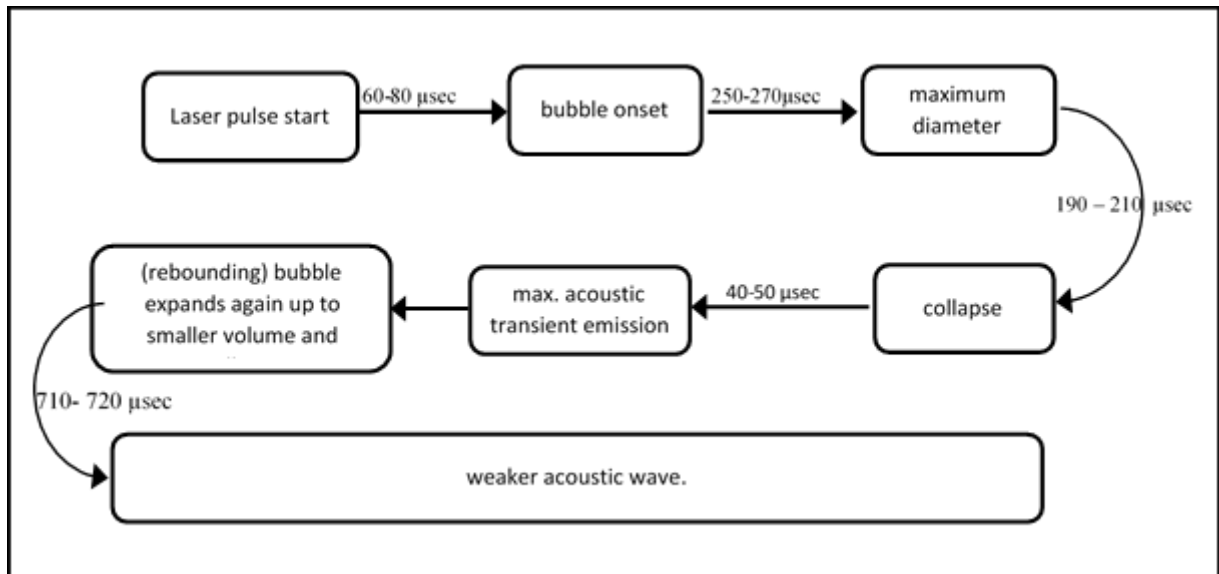


Figure.(1): The initial bubbles radii R_{bi} as a function of the fiber radii R_f for the Ho:YAG and Thulium fiber lasers.



Sketch (1): Dynamic sequence of the induced cavitation bubble stages in saline solution.

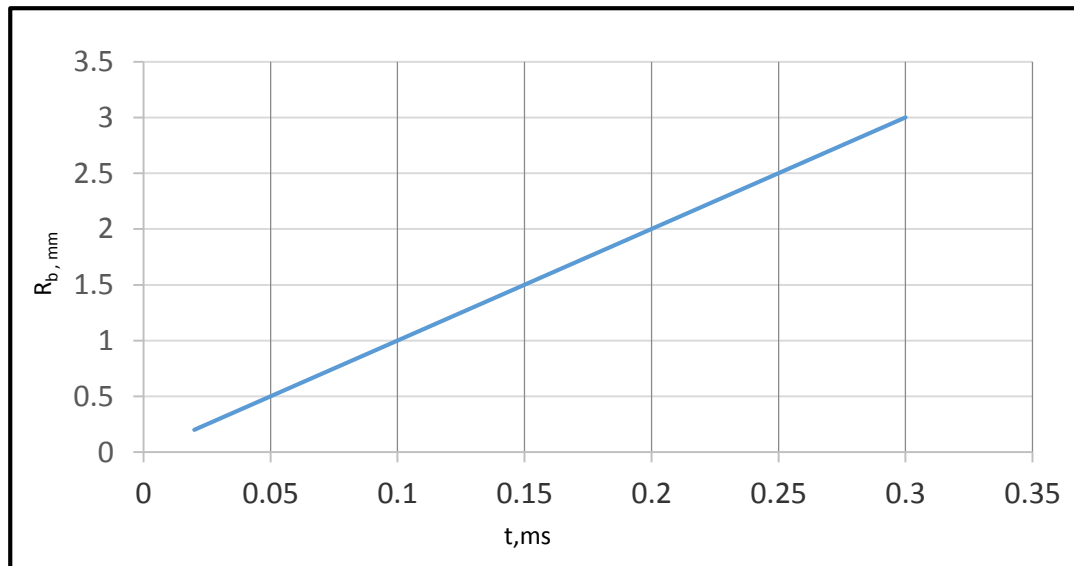


Figure. (2) The cavitation bubble radius R_b grows up with the time t , ms.

The average of the collapse transient pressure P_r was measured practically by Asshauer et.al [8]. For this reason they used a hydrophone transducer placed at 4 mm distance away from the collapse center. The changes of P_r along the distances of 1, 2, 3, 4, and 5 mm from the collapse center was calculated according to Beer-Lambert law in this study for laser energies in the range of 23.5-850 mJ passing through three different optical fiber diameters of 200, 400 and 600 micrometers. All the results are presented in figures (3, 4 and 5).

For direct presentation of the role of the optical fiber diameter alone, the calculations of the gradient change of pressure along 1-5 mm distance from the collapse center, were repeated again for a fixed 170 J/cm² fluence of the CTH:YAG laser

when delivered by three different optical fiber sizes. The presented results in fig. (6), show that the larger the fiber diameter, the higher transient pressure achieved for the same used laser fluence.

The jets impact the surface of the target calculus, tissue or the fiber face as a hammer pressure of the liquid jets and counterjets, which are related to their high speed fluid flow. This pressure was calculated using eq. (9) and the data of the published jet velocities in [20] and presented in fig. (7). They show that the hammer pressure could reaches up to more than 900 bar for jet velocity of 60 m/s.

This hammer jet pressure on the surface of the stone or on the fiber face prolonged for time duration τ depending on the initial bubble size

according to equation (10). The calculations results for the Ho:YAG and Thulium fiber types of lasers showed that this hammer jet duration is prolonged

for a very short time of up to 0.02 μ s for each jet impact as in fig. (8).

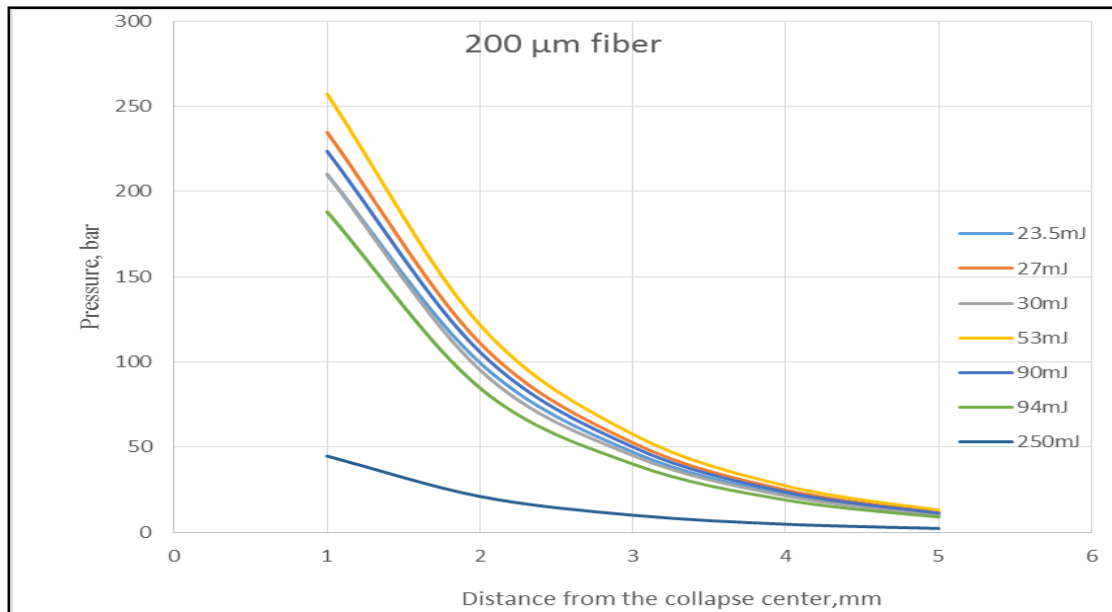


Figure. (3): The bubble collapse pressure decrease exponentially with the distance r away from the collapse center for different energies of the laser pulse passing through a 200 μ m fiber.

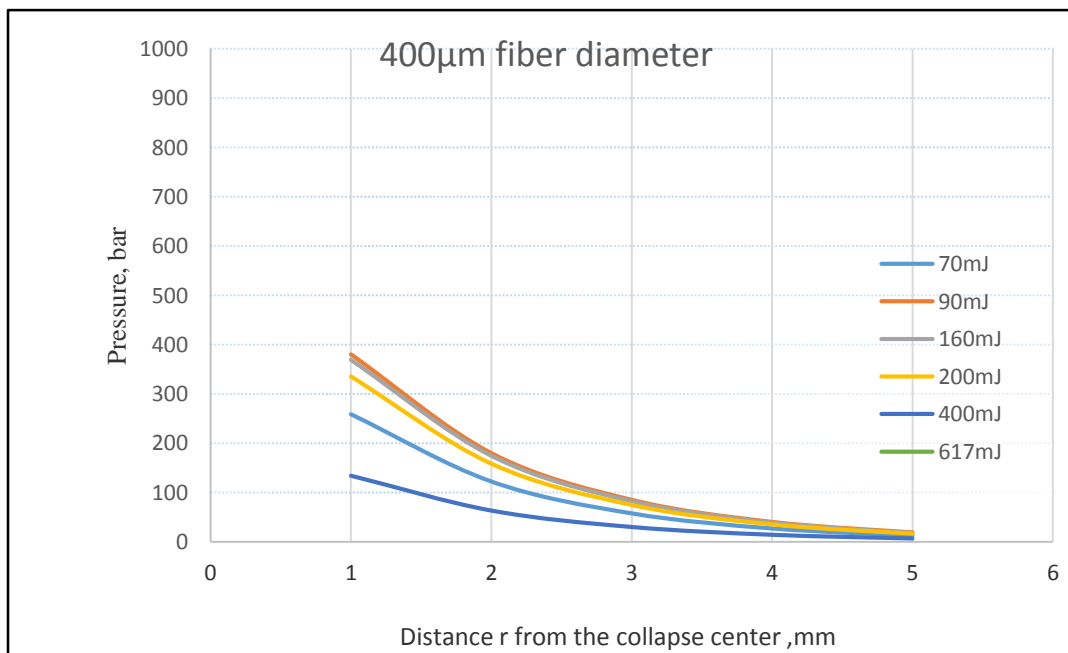


Figure. (4): The pressure due to the bubble collapse decrease exponentially with the distance r away from the collapse center for different laser pulse energies passing through a 400 μ m fiber.

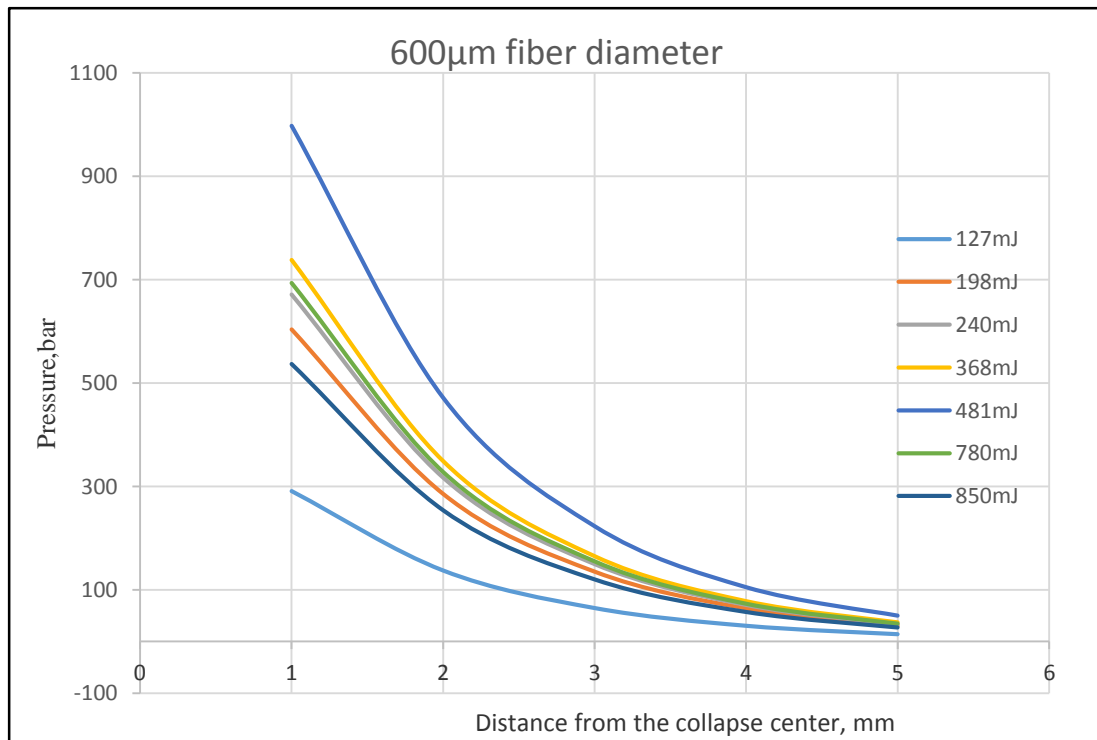


Figure. (5): The pressure due to the bubble collapse decrease exponentially with the distance away from the collapse center for different laser pulse energies passing through a 600µm fiber.

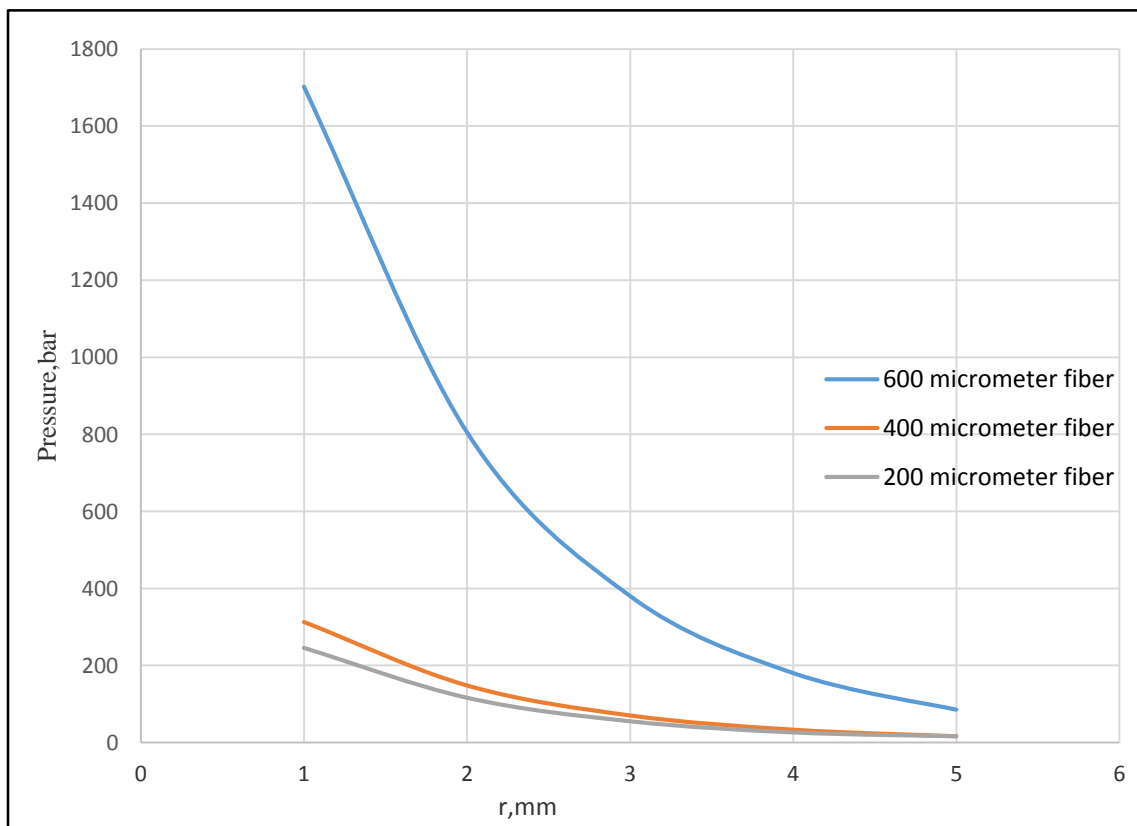


Figure. (6): The calculated pressure of the collapsed induced bubble along distance r from the collapse center. The laser fluence considered 170 J/cm² equally for the three fibers.

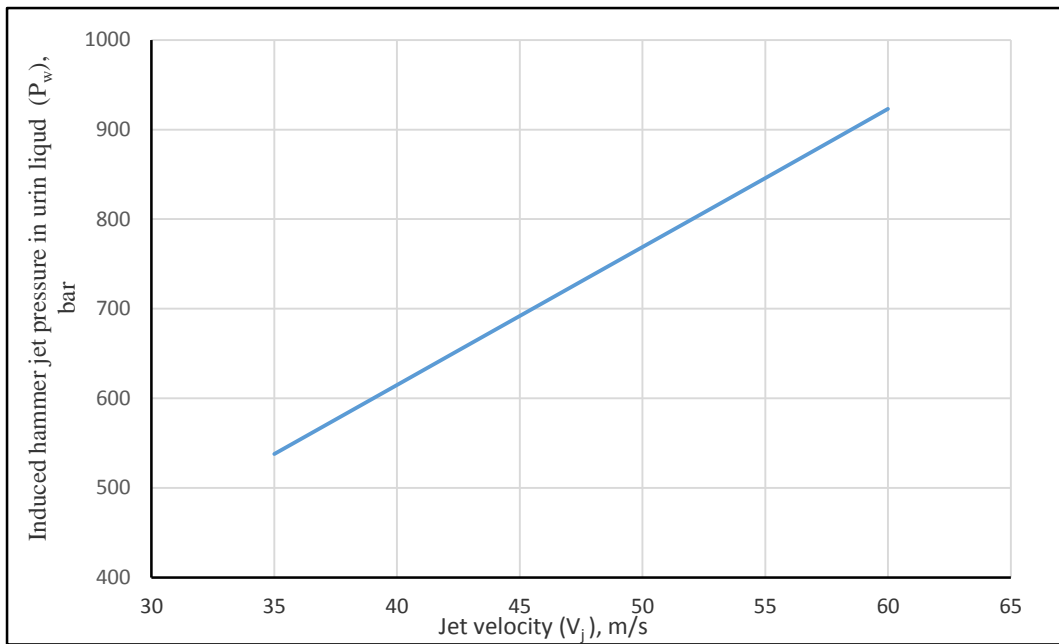


Figure. (7): The induced hammer jet pressure is proportional to the jets velocity.

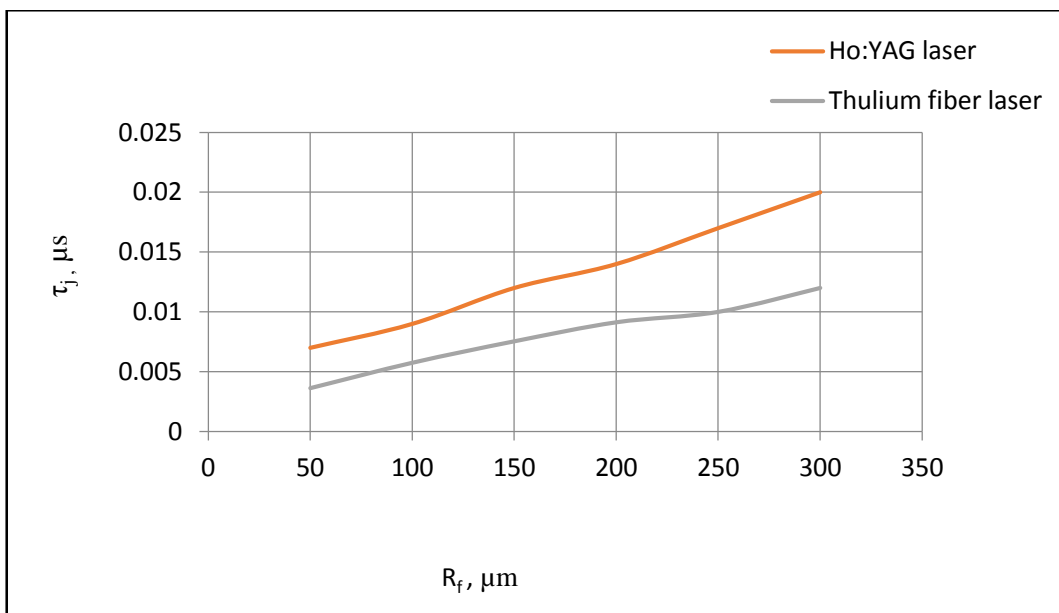


Figure. (8): The duration of the hammer jet pressure on the fiber tip face produced by the Ho:YAG and Thulium fiber lasers for different fiber sizes.

The saline with some bubbles are forced by the other bubbles collapse transient pressures to flush the very close fiber face (as well as the target) with high radial velocity U_r . The damage effect of the shearing force phenomena on the fiber face increases when it

is too close to the calculi or tissue target surfaces. The radial flow velocities U_r as a function of the bubble radius R_b were calculated for three different radial distances r (2, 4 and 6 mm) by using eq.(11). The results are shown in fig. (9).

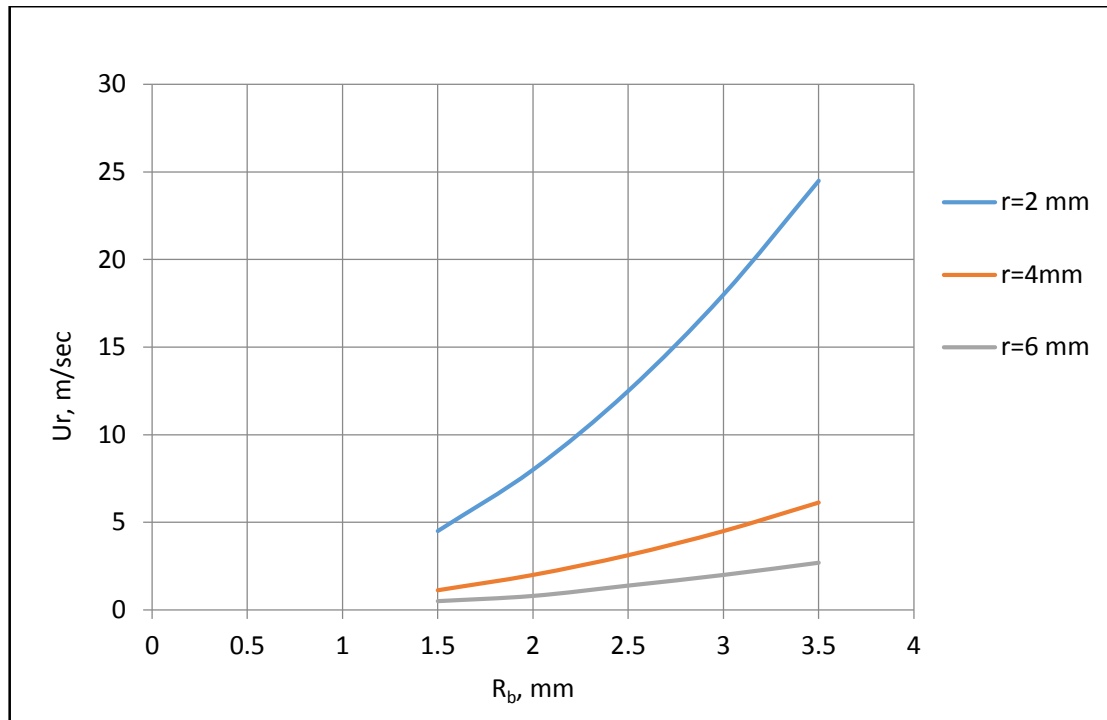


Figure (9): The bubble radial flow (flush) velocity U_r on the face of the fiber tip as a function of the bubble radius. It is inversely proportional to the radial distance r

The shearing forces on the 200 and 600 μm diameter fibers tips faces were calculated by applying the data of fig. (9) into equation (12). The viscosity of saline at temperature 100°C was considered $\approx 0.282 \times 10^{-3} \text{ N}\cdot\text{s}/\text{m}^2$ [21].

The results showed that these shearing forces on the fiber tip face for flow at radial distance $r = 2\text{mm}$ will be in the range of $(0.564\text{--}3.525) \text{ N}/\text{m}^2$ and $(0.023 - 0.141) \text{ N}/\text{m}^2$ for $r = 6\text{mm}$. The shearing forces on the face of the fiber increases when working closer to the target due to the faster radial flush flow at closer distances.

4. Discussion

The transient pressure of the collapsed bubbles propagates toward both of the target and the close to it fiber tip in the same time. The higher pressure is generated by the larger and the mostly spherical bubbles collapse rather than by the elongated shaped bubbles. As the elongated shape of the cavitation bubbles are generated by the higher laser energies, the choice of such energies reduces the ablation or fragmentation efficiency because of their lower produced transient pressure due to their non spherical shape of bubbles.

For the same operational environments, the initial bubble volume is proportional to the choice of the laser wavelength, its energy, laser pulse duration and to the diameter of the delivery optical fiber. All of these factors together determine the initial size of the generated bubbles. It was shown that for the same laser energy the use of smaller

fiber diameter leads to the generation of smaller cavitation bubbles volumes and consequently to the lower collapse transient pressure.

Due to their flow velocity and the effect of the random collapses pressures the bubbles may collide with the target surface. These collisions produce the jets and the counterjets. The jets pressures are the main effective force in tissue ablation and calculi fragmentation and even in the fiber face pitting or damage.

By referring to figs. (3, 4, 5 and 6) which show how the transient pressure is sharply decaying down and becomes weak at distances of 4-5 mm away from the collapse center and considering the earlier calculated distance of 6.72 mm to reach the maximum bubble size, it is better to hold the optical fiber at a distance of 5-7 mm away from the target during the operation. Such distance will ensure a reasonable target ablation probability, because along this distance the bubbles can have their time to grow up to their maximum volumes to produce the necessary maximum collapse transient pressure. On the same time this distance ensures the minimum damage zone for the optical fiber tip and to be far enough from the calculi fragments.

Working at such distance are more interest, for two reasons. First of them is the reduction of the fiber tip existence in the counterjets hammering strikes activities zone and second is the reduction of the shearing forces, which are produced by the

high velocity flush flow of the bubbles saline fluid on the face of the optical fiber.

5. Conclusions

The laser ablation in a liquid environment is accompanied by the bubble formation and by their mechanical effects on the fiber tip as well as on the target tissue or calculi.

The transient pressure spikes resulting from the large number of bubbles clouds collapsing near the fiber face surface over a long period of time may cause surface pitting, fatigue failure and the eventual destruction of the fiber tip end.

The fiber tip during laser ablation exposed to damage mainly first due to the compression of the new generated bubbles on the fiber tip face by the shock waves, which were produced by some elder bubbles collapse, second due to the effects of some counterjets striking the face of the fiber tip beside the shearing forces of the flush by the saline and bubbles high velocity flush flow.

Operating at very close distance allow the ejected calculus fragments to hit the fiber tip and causing its damage also.

To reduce the fiber failure chances it is recommended to use the 200 μ m and micro seconds laser pulses besides keeping an optimum distance of 5-7 mm between the fiber tip and the target. Then the operating life of the fiber could be prolonged with the insurance of a good ablation efficiency.

6. References

- [1] A.J. Welch, H. W. Kang, H. Lee, J. M. H. Teichman, "Calculi fragmentation in laser lithotripsy", *Minerva UrologicaNefrologica*, vol.56, no.1, (2004), p 49-63.
- [2] R. Hofmann, R. Hartung, H. Schmidt-Kloiber, and E. Reichel, "Laser-Induced Shock Wave Lithotripsy. Influence of laser pulse energy and irrigation solutions on stone disintegration", *Urological Research*, 18, Springer-Verlag, (1990), pp 45-48.
- [3] T. Asshauer, G. Delacretaz, "Analysis of fiber damage risk during pulsed holmium laser application under water" *Laser in medical science*, 12,(1997), pp 157-163.
- [4] Nathaniel M. Fried, Richard L. Blackmon, Pierce B. Irby, "A review of Thulium fiber laser ablation of kidney stones", *Proc. Of SPIE* Vol.7914, (2011). 791402-1
- [5] Kin Foong Chan, Bernard Choi, Gracie Vargas, Daniel X. Hammer, Brian Sorg, T. Joshua Pfefer, Joel M. H. Teichman, Ashley J. Welch, E. Duco Jansen, "Free Electron Laser Ablation of Urinary Calculi: An Experimental Study", *IEEE Journal on Selected Topics in Quantum Electronics*, Vol. 7, NO. 6, November/December, (2001).
- [6] Ton G. Van Leeuwen, E. Duco Jansen, Ashley J. Welch, Cornelius Borst, "Eximer laser induced bubble: Dimensions, theory and applications for laser angioplasty", *Laser in surgery and medicine*, 18, (1996), pp 381-390.
- [7] Markolf H. Niems, "Laser tissue interactions" *Springer*, (2002), pp 143-149.
- [8] T. Asshauer, K. Rink, G. Delacretaz, "Acoustic transient generation by Holmium-laser-induced cavitation bubbles" *J. Appl. Phys.* 76 (9), November, (1994), pp. 5007-5013.
- [9] R. A. London, D. S. Bailey, P. Amenda, S. Visuri, V. Esch, "A Scaling model for laser-produced bubbles in soft tissue" *SPIE international symposium on bios'98, proceeding SPIE digital library* Vol. 3254, (1998), pp.256-263.
- [10] Peter Gregorčič, Matija Jezeršek, Janez Možina, "Optodynamic energy-conversion efficiency during an Er:YAG - laser-pulse delivery into a liquid through different fiber-tip geometries" *Journal of biomedical optics*, 17 (7), July,(2012), pp 75006 1-8 .
- [11] Reinher Pimentel-Dmi'ngues, Jaun Herna'ndez-Cordero, Roberto Zenit, "Microbubble generation using fiber optics coated with nanoparticles" *Optics Express*, Vol. 20, Issue 8, (2012), pp.8732-8740.
- [12] Fre'dre'c Caupin, Eric Herbert, "Cavitation in water: a review" *Comptes Rendus Physique*, Elsevier, (2006), pp. 1000-1014.
- [13] C.M. Christian, E.G. Paterson, A.A. Fontaine, "Modelling laser-generated cavitation bubbles", 18th Australasian fluid mechanics conference, Australia, (2012).
- [14] Wayne Kreider Chen, Hong Chen, Michael R. Bailey, Andrew A. Brayman, Thomas J. Matula "Potential mechanism for vessel invagination caused by bubble oscillations", *IEEE International ultrasonic symposium proceedings*, (2009), pp. 353-356.
- [15] Alfred Vogel, "Nonlinear absorption: intraocular microsurgery and laser lithotripsy", *Phys. Med. Biol.*, 42, (1997), pp. 895-912.
- [16] Alfred Vogel, Vasan Venugopalan, "Mechanisms of Pulsed Laser Ablation of Biological Tissues", *Chemical Reviews*, American Chemical Society, Vol. 103, No.2, (2003), pp. 623-635.

[17] Olger Lindau, Werner Lauterborn, "Investigation of the counterjet developed in a cavitation bubble that collapses near a rigid boundary", Drittesphysikalisches institute, UniversitätGöttingen,Germany, (2001), pp 1-7.

[18] Claus-Dieter Ohl, Thomas Kurz, Reinhard Geisler, Iger Lindau, Werner Lauterborn, "Bubble dynamics, shock waves and sonoluminescence" The royal society, 357, (1999), pp. 269-294.

[19] E. A. Brujan, P. R. Willaims, "Bubble dynamics and cavitation in non-newtonian

liquids", Rheology review, The British society of rheology, (2005), pp. 147-172.

[20] T. Kodama, Y. Tomita, "Cavitation bubble behavior and bubble-shock wave interaction near a gelatin surface as a study of in vivo bubble dynamics" Appl. Phys.B, laser and optics, (2000), pp. 139-149.

[21] John J. Bloomer, "Practical fluid mechanics for engineering applications" Marcel Dekker inc., N. Y., 2000, pp. 9-12.

دراسة حسابية وتحليل للاضرار الميكانيكية التي تهدد طرف الليف البصري أثناء العمليات الجراحية بالليزر

منقذ سليم داود

قسم الهندسة الطبية
كلية الهندسة / جامعة النهريين

الخلاصة:

لوحظ وجود تضرر في اطراف الالياف البصرية المستخدمة في تطبيقات الجراحة الطبية بالليزر التي تجري في الوسط المائي المحيط بمنطقة العمل كما في عمليات الناظور وتفتيت حصى المجاري البولية. وقد درست ظاهرة توليد الليزر للفقاعات المجوفة ومايصاحبها من تأثيرات ميكانيكية على طرف الليف البصري الناقل لاشعة الليزر خلال اجراء هذه العمليات. ووضحت النتائج انه بسبب انهيار هذه الفقاعات يتعرض راس الليف البصري الى تأثير الضغط الذي يولد هذا الانهيار اضافة الى ظهور ضربات مطرقية وقوى قطع ميكانيكية بسبب السرعة الكبيرة لجريان هذه الفقاعات. وتم حساب هذه القوى الميكانيكية المتكررة المؤثرة على راس الفايبر لثلاثة احجام فايبر اتبصرية مختلفة ووضحت النتائج انه لاجل تقليل الاضرار الناتجة يفضل استخدام الفايبرات الاقل حجما مثل التي قطرها 200 مايكروميتر وان يتم اجراء العملية الجراحية بحيث يمسك الفايبر ليكون راسه على بعد 5-7 مللمتر من النسيج أو الحصوة المطلوب معالجتهما لاطالة عمر عمل الفايبر مع الحفاظ على كفاءة عملية القطع في الوقت نفسه.

الكلمات المفتاحية: تضرر الليف البصري, الفقاعات المجوفة, ديناميك الفقاعات, النفثات المطرقية.